Eidgenössische Technische Hochschule Zürich
Swiss Federal Institute of Technology Zurich

Laboratory for High
Power Electronic Systems

Semester Project

Development of a Magnetic Levitating System for the Swissloop Pod

Giacomo Burani

February 18, 2023

Supervisor: Beglinger Lars
Professor: Prof. Dr. Jürgen Biela

Abstract

The Hyperloop concept proposes a new method of transport that is comparable to trains and buses in terms of energy efficiency and comparable to air crafts in terms travelling speed. The Swissloop team at ETH Zürich is a student team that continuously innovates the Hyperloop technology by building a pod and improving it each year. This thesis contributes to the improvement of the Swissloop pod by replacing the suspension and the guidance wheels with a magnetic levitation suspension with a focus on the development and design of a control system for the magnetic levitation and guidance for the pod. The proposed control system is designed to ensure stability, accuracy and safety of the levitation process. The system is modelled and the methodologies used to design, test and validate the control system with simulations in the Matlab SIMULINK environment. The analyzed performance metrics are the ability of the control system to levitate at a constant height above the rail by rejecting possible disturbances, the smoothness of the ride, and power usage to levitate. The control system is shown to be stable in the simulation under varying operating conditions such as added noise to the position sensor signal, track misalignment, bent tracks, and presence of disturbance forces. It suggests a slightly bigger levitating range to account for the effects of the noise, thus emphasizing the importance of good noise-filtering techniques.

Acknowledgements

First of all, I would like to express my sincere gratitude to Prof. Dr. Jürgen Biela for the opportunity to perform my Semester Project at the laboratory for High Power Electronic Systems (HPE).
Then, I would like to thank Lars Beglinger for his supervision and the feedback he gave me throughout the whole duration of this project.
Finally, I want to thank the whole Swissloop team for the opportunity of being part of this important project and innovative team.

Nomenclature

Acronyms and Abbreviations

MagLev	Magnetic Levitation
EMS	Electromagnetic Suspension
EDS	Electrodynamic Suspension
LIM	Linear Induction Motor
LSM	Linear Synchronous Motor
HEMS	Hybrid Electromagnetic Suspension
EMF	Electromotive Force
DOF	Degree of freedom

Symbols

N	Number of windings	[−]
μ_0	Magnetic permeability of free space	[$\mathrm{N\,A^{-2}}$]
F	Force	[N]
I	Current	[A]
B	Magnetic field density	[T]
H	Magnetic field	[$\mathrm{A\,m^{-1}}$]
δ	Air gap	[m]
Θ	Electromotive Force	[A]
h_d	Permanent magnet thickness	[m]
A	Cross sectional area	[$\mathrm{m^2}$]
l_{Fe}	Electromagnet core length	[m]
t	time	[sec]

Project Definition

Description

Dates

Beginning:	September 26, 2022
End:	December 23, 2022
Final presentation:	February 10, 2023
Deadline for report:	January 18, 2023

Supervisor

Lars Beglinger, ETH, beglinger@hpe.ee.ethz.ch

Professor

Prof. Dr. J. Biela

Development of magnetic levitating system for the Swissloop pod

Semester Project

Professor:	J. Biela
Supervisor:	L. Beglinger
Starting date:	tbd
Duration:	240h (8 ETCS)
Grading criteria:	According to HPE grading sheet

1. Objectives

The objective of this semester project is to lay the foundations for the implementation of a magnetic levitation controller on the Swissloop pod. In order to properly implement the controller in the real system, an accurate model of both the real system and the controller need to be available to test for theoretical stability and dimensioning the system.

2. List of Assignments

1. **Literature review:** Focused on magnetic levitation and control theory.
2. **Electromagnetic Testing:** Testing the electromagnetic components to allow for a more accurate modelling of the system.
3. **Model development:** Formulation of the equations for the electromagnetic circuit and model development (MATLAB, Simulink or other agreed-upon software).
4. **Performance assessment:** Development of a theoretical controller (PID, LQR or other agreed-upon type) and assessment of basic performance indicators (stability, reaction speed, settling time,…).
5. **(Seminar)**
6. **(Report)**

Contents

Chapter 1

Introduction

1.1 Motivation

The transportation sector has been identified as one of the major contributors to climate change [1], with greenhouse gas emissions accounting for 16.2 % of global emissions in 2020. The road transport sector alone accounted for 11.9 % of emissions, while aviation and rail accounted for 1.9 % and 0.4 % respectively [2]. While from the emission data trains seems to be a more energy-efficient mode of transport, a fair comparison must also take into account other factors such as energy intensity. Otherwise the differences in emissions could be caused by the different penetrations of the respective technologies.

To make a fair comparison, it is important to introduce an appropriate efficiency unit. In this thesis, the units of energy per passenger-kilometers (MJ/pkm) for passenger transport is used and energy per tonnes-kilometers (MJ/tkm) for freight transport. The energy intensity of various modes of transport can then be defined as follows:

$$\text{Passenger energy intensity} = \frac{\text{Energy consumption (MJ)}}{\text{Passengers-kilometers (pkm)}} \tag{1.1}$$

while for fright transportation is

$$\text{Freight energy intensity} = \frac{\text{Energy consumption (MJ)}}{\text{Tonnes-kilometers (tkm)}} \tag{1.2}$$

Table 1.1: Energy consumption parameters and features for different transportation modes [3]. The energy consumption is calculated according to (1.1)

Mode	**Seats**	**Occupancy** (%)	**Energy consumpt.** (MJ/seat km)	**Energy consumpt.** (MJ/pkm)
Hyperloop	-	-	0.14-0.63 [4, 5]	-
Heavy rail	555	15	0.25	1.69
Standard bus	48	33	0.34	0.92
Rail electric and diesel	377	28	0.45	1.65
Car	4	50	0.92	2.1
Air Boeing 727	167	60	1.45	2.42

Although trains are considered one of the most energy-efficient modes of transportation,

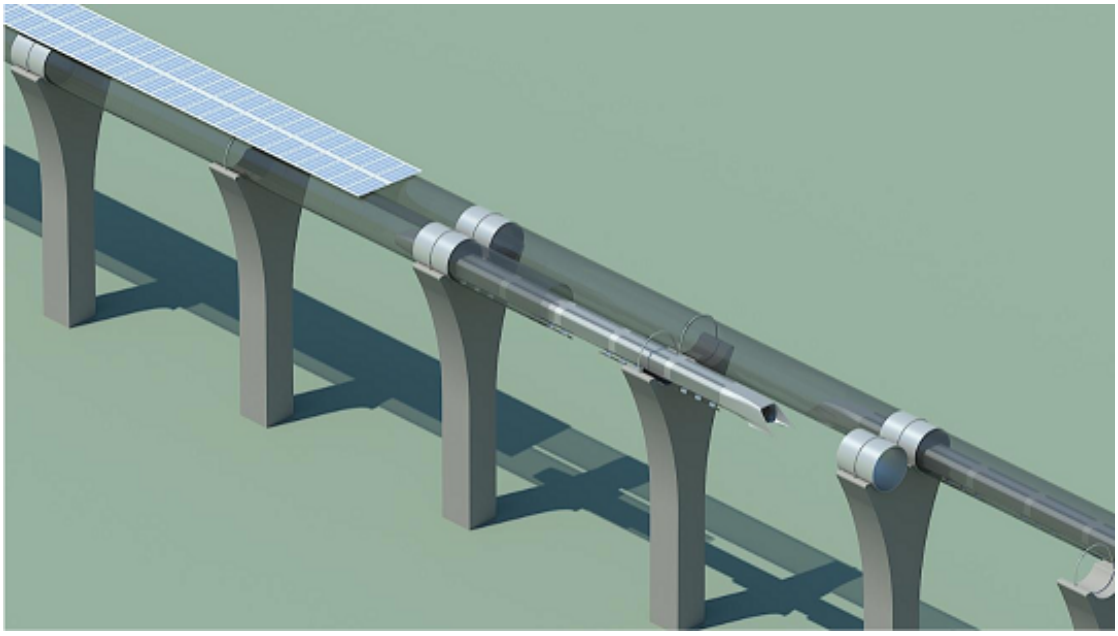

Fig. 1.1: Sketch of Hyperloop concept [7]. The capsule with the passenger/cargo travels inside tubes under near vacuum condition placed on top of pillars. Ideally the capsule levitates above the rail to allow for higher speed and less wear due to friction.

as it can be seen in Tab. 1.1, they still have limitations in certain areas. For example, in terms of speed, air travel is often the faster option, with today's commercial flight speeds averaging between 740-930 $\mathrm{km\,h^{-1}}$, compared to high-speed trains which typically have speeds in the range of 160-300 $\mathrm{km\,h^{-1}}$. Additionally, trains and planes also contribute to noise pollution both within and outside of urban areas. In the case of trains, this problem is present during the whole operation duration while air transport only has an impact during takeoff and landing. Long-term exposure to noise above certain levels has been linked to various health complications such as sleep disturbance, effects on the cardiovascular and metabolic system, cognitive impairment in children, and annoyance [6]. A better overall transport method should therefore be at least as fast as an aircraft, quieter than a train and more energy efficient than both. Such a transport design can be found in the Hyperloop concept, which proposes to transport passengers and cargo in a low-pressure tube, reducing the density of the medium and thus the drag force. This technology, which could potentially revolutionize the way passenger transport is conceptualized, is introduced in the next section.

1.2 Hyperloop Concept

The general concept of the Hyperloop technology is to reduce the air drag resistance of the transport vehicles to achieve higher speeds than conventional method of transport by

operating in a controlled environment under near vacuum conditions. This is achieved by operating passenger capsules inside of tubes placed either on the ground or on pylons above the ground. The motivation behind this choice is that air resistance is one of the main reasons behind the limited speed of conventional vehicles [8]. The drag power loss experienced by a body moving through a medium, such as air, can be expressed by the equation:

$$P_{\mathrm{D}} = F_{\mathrm{D}} \cdot V = C_{\mathrm{D}} A \frac{\rho V^3}{2} \tag{1.3}$$

Where F_{D} is the drag force, C is the drag coefficient, A is the cross sectional area, ρ is the density of the medium and V is the velocity of the body. It is evident that the drag power loss scales with the third power of the velocity and proportionally to the density of the medium. Therefore, to achieve higher speeds while keeping the power losses within acceptable limits, it is necessary to either significantly decrease the drag coefficient, which is challenging due to the already optimized shape of the train, or to reduce the cross sectional area of the train, although a smaller cross section could cause other problems such loss of passenger comfort or loss of storage room. Another way to decrease the drag force is to travel through a less dense medium. This is also the reason why planes travel at high cruise altitudes where the air resistance is lower due to lower air density, allowing them to travel faster and use less fuel. The Hyperloop concept is therefore meant to be

- With a speed comparable to that of planes and easier boarding
- Quieter than planes and trains
- Not interfering with the other vehicles along the route like cars and busses
- More energy efficient than trains
- Not using fuel to propel and relying on electricity instead, which could potentially have a significant positive impact on greenhouse gas emissions, provided that the electricity is produced sustainably

This technology gained popularity after 2013 Tesla's white paper [7]. The paper suggests this new concept as a substitute to the expensive California "High speed" rail [7]. In the authors opinion, the near vacuum conditions are preferred to hard vacuum because of the possible presence of leaky seals or small cracks that would lead the whole system to a stop. Instead, by operating at low pressures, at a level sustainable for commercials pumps, the system is able to overcome the aforementioned leakage problems [7].

Another feature of this design that allows for high speeds comparable to planes is substituting conventional wheels with some kind of non-contact suspension, such as magnetic levitation or air bearings, thus eliminating power losses to friction and instabilities occurring in the wheels and axles at transonic cruising velocities. This feature is already present in magnetic levitation (maglev) trains design, which exploit magnetic levitation to suspend the train above the rails.

1.3 Maglev trains

The use of magnetic levitation technology in trains has been proposed as a solution to address noise pollution issues [9, 10], as it eliminates the contact between the train and the rails, which is one of the main sources of noise for traditional rails. There are currently two types of maglev trains in service: Electromagnetic suspension (EMS) and Electrodynamic suspension (EDS)[11]. EMS utilizes an electromagnet placed below the rail and fixed to the train structure to attract the train upwards towards the magnets attached to the rails. On the other hand, EDS uses permanent magnets to repel the train from the guide-way, typically utilizing super-cooled and superconducting magnets to achieve levitation heights of about 10 cm. It is important to note that while EDS technology provides a higher levitation height, it is slower to lift off, requiring the use of safety wheels at speeds below $100\,\mathrm{km\,h^{-1}}$.

The levitation principle allows for a number of advantages, such as a quiet operation, smooth ride for passengers, and a reduced likelihood of derailment. Furthermore, compared to traditional trains, maglevs have lower operating and maintenance costs, as the absence of rolling friction leads to less wear and tear on parts and less energy loss through friction forces. Additionally, the lack of friction enables maglev trains to achieve extremely high speeds, with some reaching more than 500 $\mathrm{km\,h^{-1}}$ (Shinkansen L0 Series).

In most applications, once the train is levitated, it is propelled forward using a changing phase electric motor. A normal electric motor uses a magnetic field to generate torque on an axle, comprising of a stationary part called the stator, which generates the magnetic field, and a rotor, which is subject to the magnetic field from the stator. To achieve propulsion, instead of torque, the circular stator is conceptually unrolled into a long flat surface and the rotor is propelled forward instead of spinning it. In this case the rotor does not rotate and it is therefore called secondary, while the stator becomes the primary.

The field generated by the stator on the pod produces a propelling force on the tracks, i.e. the secondary. This is known as a Linear Induction Motor (LIM). However, there is a loss of energy and speed due to the secondary lagging behind the primary's moving magnetic field. To address this issue, the concept of a Linear Synchronous Motor (LSM) is introduced. In a LSM design, a permanent magnet is attached to the secondary, allowing it to produce its own magnetic field which travels in sync with the stator's moving magnetic field [11]. Regarding guidance, which address the problem of keeping the maglev centered on track, there are two solutions. The first guidance system, developed as part of the TransRapid concept [12], utilizes two electromagnetic rails placed on the side of the train facing either side of the guide-way. This system uses the electromagnetic force generated by the rails to keep the train centered on the track. The second guidance system, found in the MLX design [12], is integrated with the levitation system. This system uses two levitation rails placed on either side of the train and connected to each other. When the train moves towards one side, a restoring force is passively induced which moves the train back to the center[12].

1.3.1 Swissloop

The Hyperloop and maglev concepts, when combined, could create a revolutionary transportation method that surpasses traditional methods in terms of speed, noise reduction, and efficiency. The Hyperloop addresses the issue of air drag and maglevs eliminate friction drag and noise. Therefore a lot of research has been devoted to this topics and a lot of engineering teams have been founded in universities across the world to present a proof of concept, and evaluate their achievements and progresses in annual competitions that tests all the aspects of their proposed design. One of the leading teams in this field is the Swissloop team form ETH Zürich, who ranked highly in all the competitions they took part of. This team builds a scaled down capsule prototype following the hyperloop concept, the so called pod. They innovate and improve their design every year, and operate and test it on a rail track. Since the team was founded, propulsion has been generated using a modification of a LSM motor design and the pod was either suspended using wheels or passive magnetic levitation exploiting the magnetic field of the motor. In recent years, the team switched to a new design for the propelling electrical motor which do not allow passive levitation anymore. Therefore, this work will focus on the design and testing of magnetic levitation for the Swissloop pod.It is expected to reduce the energy loss due to friction, as well as overcome the speed limitation imposed by the employment of conventional wheels. Moreover, passive guidance is not possible anymore due to the new motor type and for this reason a possible guidance system design for the Swisslop pod is proposed.

Chap. 2 provides a thorough theoretical background of the control system, which includes an overview of the principles of magnetic levitation, dynamics, a description of the control system architecture, and a discussion of the control algorithms used to ensure the stability and accuracy of the levitation process.

Chap. 3 is dedicated to the methodology used to evaluate the controller's performance using SIMULINK simulations. This includes a description of the system modeling process, the operating conditions, and the performance metrics used to evaluate the control system. The section also includes a detailed analysis and discussion of the simulation results, which demonstrate the effectiveness of the proposed control system in maintaining the stability of the levitation system and improving the tracking performance.

Finally, the thesis concludes with a summary of the main results, highlighting the key contributions of the study, and suggesting directions for future research. The conclusion emphasizes the importance of this work in advancing the Hyperloop technology and the potential of the proposed control system to enhance the performance, safety, and efficiency of the levitation process.

Chapter 2

Theory

This chapter presents the main equations used for the modelling of the proposed levitating system. The general analysis of the electromagnetic circuit is introduced to determine the electromagnetic force equation. Moreover a section on the analysis of the time constant of the system is presented as well as a brief introduction to the control system theory necessary to better understand the chosen controller structure.

2.1 Electromotive Force (EMF)

The chosen concept for the vertical levitation system is a hybrid electromagnetic suspension system (HEMS), so that the permanent magnets are able to compensate the constant weight force of the pod and the electromagnetic component is responsible for handling disturbances. In the case of the lateral guidance there is no DC offset, therefore a simple electromagnetic suspension (EMS) is used. The modelling of the HEMS should also account for the magnetic flux generated by the permanent magnet. In order to derive the correct equation for the electromagnetic force of the EMS/HEMS, an analysis of the magnetic circuit is conduced [13]. For the following derivation the following assumptions are made

- The permanent magnets have a linear DC magnetization curve and no hysteresis
- No leakage flux and ideal ferromagnetic material
- The reluctance of the iron core and permanent magnet is negligible compared with the reluctance of the air, i.e. $H_{\mathrm{Fe}} \cdot l_{\mathrm{Fe}} \approx 0$
- Permanent magnet and electromagnet have the same constant cross sectional area A
- The relation between magnetic field density B, magnetic field H and magnetic permeability of the material μ is linear and it is expressed by

$$B = \mu H \tag{2.1}$$

These assumptions allow for a first rough modelling of the complex system. This analytical model allows to test the control structure in the early stages of the project, and will be then substituted in the controller tuning phase by look up tables with numerical

simulations data once the final design of the HEMS/EMS is fixed. The electromagnetic force is found using

$$F_{\text{mech}} = \frac{1}{2} I_1^2 \frac{\partial L(\delta)}{\partial \delta} \tag{2.2}$$

where I is the current in the coil, L is the inductance of the coil and δ is the air-gap distance. Using the assumptions, this equation reduces to

$$F_{\text{mech}} = \frac{B^2 A}{\mu_0} \tag{2.3}$$

where B is the magnetic flux density and μ_0 the magnetic permeability of free space. In both the EMS and the HEMS system the magnetic field density B is found usign the reluctance model

$$\begin{aligned} \Theta &= NI \\ &= \sum_v V_v \\ &= \sum_v H_v l_v \end{aligned} \tag{2.4}$$

where Θ is the magneto-motive force, V represent the magnetic voltage and l_v is the longitudingal length of the material v.

2.1.1 Vertical Levitation

For the case of the HEMS, it is important to account for the permanent magnets when analyzing the magnetic circuit, which, using (2.4), can be expressed as

$$\begin{aligned} \Theta &= V_m + V_{\text{Fe}} + V_L \\ &= H_m h_D + H_{\text{Fe}} l_{\text{Fe}} + 2 H_L \delta \end{aligned} \tag{2.5}$$

where Θ is the magneto-motive force, N is the number of winding and V represent the magnetic voltage. By combining eqs. (2.1), (2.3) and (2.5) together, and thanks to the assumption that the reluctance of the air gap is much bigger than that of the iron, the mechanical force exercised by the HEMS is given by

$$\begin{aligned} F_{\text{mech}} &= \frac{(NI - H_{\text{m}} h_D)^2 A}{(\frac{l_{\text{Fe}}}{\mu_{\text{Fe}}} + \frac{2\delta}{\mu_0})^2 \mu_0} \\ &= \frac{(H_{\text{m}} h_D - NI)^2 A \mu_0}{4\delta^2} \end{aligned} \tag{2.6}$$

For simulation purposes, the quantity $H_{\text{m}} h_D$ is substituted with an equivalent electromagnetive force $(NI)_{eq}$. This last step simplified the simulations assuming the magnetic field produced by the permanent magnet as constant. As shown in Chap. 3, despite this

assumption, the analytical model and the COMSOL simulations yields similar results. It is important to note that the HEMS system is designed such that the electromagnet is able to both weaken and strengthen the permanent magnet's field. When the electromotive force (EMF) of the coil is the same as the EMF of the permanent magnet $(NI)_{eq}$, the resulting force is zero [13]. This value represents the positive limit of the flux generated by the coil, such that when the current is at its maximum the produced force is zero. In the case of a negative current, the EMF of the permanent magnet works alongside with that of the electromagnet and strengthens it.

2.1.2 Lateral Stabilization

For the lateral movement, a simple EMS is used. Therefore, (2.5) reduces to

$$\Theta = H_{\text{Fe}} l_{\text{Fe}} + 2H_L \delta \tag{2.7}$$

and, using (2.1), the mechanical force by the electromagnet is equal to

$$\begin{aligned} F_{\text{mech}} &= \frac{(NI)^2 A}{(\frac{l_{\text{Fe}}}{\mu_{\text{Fe}}} + \frac{2\delta}{\mu_0})^2 \mu_0} \\ &= \frac{(NI)^2 A \mu_0}{4\delta^2}. \end{aligned} \tag{2.8}$$

2.2 Rise Time

The considered system is highly dynamic and the response time needs to be assessed to assure stability and safety in operation. It is therefore necessary to compare the time constant of the dynamics of the system with the time constant of the current reaction.

To control the current, Swissloop uses inverters, and simulations show that the current rise time inside the electrical circuit can be linearly approximated using

$$\frac{\partial I(t)}{\partial t} \approx \frac{U}{L} \tag{2.9}$$

where U is the voltage and L the inductance of the coil. From (2.9) it is easy to derive the time delay

$$t_{\text{delay}} = \Delta I_{\text{goal}} \frac{U}{L} \tag{2.10}$$

where ΔI_{goal} is the wanted current step starting from the current in the circuit at that moment. Given that the inductance is also dependent on the air gap, to calculate the circuit delay, an air gap distance corresponding to the equilibrium distance is used.

To calculate the dynamics time constant, a free fall approach is used. It is calculated by looking at how much time it takes for the pod to reach the maximal allowable displacement starting from the equilibrium position when the maximal force is applied, denoted as δ_{eq}. To simplify the calculations, the dynamics of the system in (3.8) are discretized and the

acceleration of the system is considered constant over the discretization time interval $\mathrm{d}T$

$$\ddot{z}(T) = -g + \frac{(H_\mathrm{m} h_\mathrm{D} - NI)^2 A \mu_0}{4(\delta_\mathrm{eq} - z(T))^2 m} \qquad \text{for } T < t < T + \mathrm{d}T \tag{2.11}$$

Considering the acceleration as a constant over the period $[T, T + \mathrm{d}T]$ allows to write the vertical displacement dynamics as follows

$$z(T + \mathrm{d}T) = z(T) + \dot{z}(T)\mathrm{d}T + \frac{1}{2}\ddot{z}(T)\mathrm{d}T^2. \tag{2.12}$$

This way it is only necessary to look at the time it takes the system to surpass the maximal displacement $\delta_\mathrm{eq} + z_\mathrm{max,displ}$ and that time would be the time constant of the system dynamics. To be consistent in comparing the two time constants, electrical circuit delay and dynamics delay, the worst case scenario is assumed. It is considered the case where the pod is free falling and the current need to be switched from 0 A to I_max in order to counteract the free fall. This switch should in fact be faster than the time it takes the system to fall for the maximal displacement allowable, which is precisely the dynamics time constant calculated using (2.11). If $t_\mathrm{delay,el} \ll t_\mathrm{delay,dyn}$ then the electromagnet is able to react fast enough to react to pod displacements and stabilize it. To help this comparison, the variable r_delay representing the ratio between the two time constants is introduces as

$$r_\mathrm{delay} = \frac{t_\mathrm{delay,el}}{t_\mathrm{delay,dyn}} \tag{2.13}$$

Only the worst case scenario is considered for the current build-up because the delay scales linearly with the ΔI_goal. Therefore, if it is necessary to make smaller adjustment, the electrical circuit will react even faster.

2.3 Control-loop basics

In order to maintain a desired range of operation, the output of a dynamic system often requires control through the use of inputs. There are two main types of control methods: open-loop and closed-loop. A controller sends input to the system, known as the plant, which then produces an output based on the input received. In closed-loop control, the input is determined by the current state of the system, while in open-loop control, the input is predetermined and not based on the current state of the system. While open-loop control may be simple and inexpensive, closed-loop control offers a clear advantage due to its ability to correct for external disturbances. In closed-loop control systems, a feedback loop continuously sends information from the output to the controller. The output is compared to a reference value, or the desired operating point, and any difference between the two, known as the error, is used by the controller to bring the output closer to the reference. This is not possible in open-loop control, where external disturbances can cause significant deviations from the expected outcome. A common structure of a closed-loop

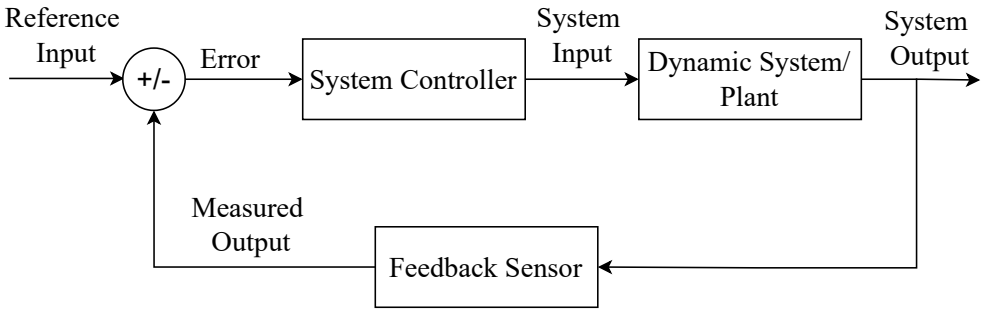

Fig. 2.1: General structure of a closed loop control structure [14]. The controller allows to regulate the output of the system according to the error between the reference and the real output, sending inputs to the plant to reduce it.

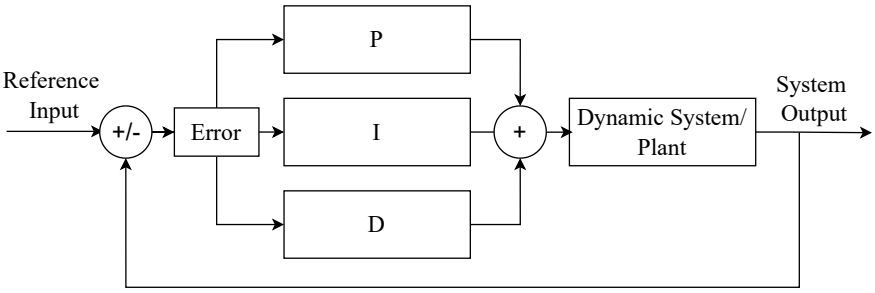

Fig. 2.2: General structure of a PID controller [14]. In this figure the three components of the controller are a visibly separated: proportional, integral an derivative. These parameter are easily tunable, thus making the PID a very versatile controller type, and put emphasis of different aspects on the behaviour of the error function.

control system is shown in Fig. 2.1.

For the complex and unpredictable Swissloop pod system, a PID controller is the most suitable choice due to its versatility and ease of tuning. The structure of a PID controller is shown in Fig. 2.2 and it operates by adjusting the output of the system based on the behavior of the error function. This controller is divided into three parts: proportional, integral, and derivative. The output is calculated by combining the contributions of these three parts. The proportional part responds to the current error, the integral part accounts for past errors, and the derivative part predicts future errors. Together, these components enable the PID controller to effectively regulate the output of the system, which is calculated using

$$y(t) = K_\mathrm{p} e(t) + K_\mathrm{i} \int e(t)\mathrm{d}t + K_\mathrm{d} \frac{\mathrm{d}e(t)}{\mathrm{d}t} \tag{2.14}$$

where $e(t)$ is the error function defined as $e(t) = r - y(t)$, and $y(t)$ is the output of the system. K_p, K_i and K_d are the tuning parameters responsible for scaling different aspects

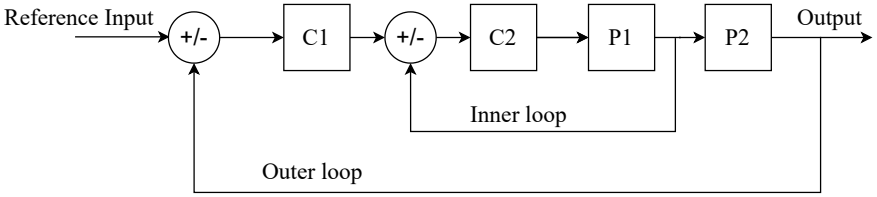

Fig. 2.3: General structure of a cascade PID controller[14]. This control structure allows to control system where there are two or more interconnected quantities to control that change at different rates. It presents an inner control loop, which allows to control faster changing variable with C_2, and an outer control loop, responsible for controlling variables that vary at a slower rate with C_1.

of the error function. They are able to put more emphasis on either the absolute distance from the reference, the rate of change of the output or the long term behaviour of the error function. Additionally, to optimize the control system for the levitation problem of the Swissloop pod, it may be necessary to modify the structure of the loop. In this specific case, the control system is divided into two smaller control systems. One system, the current-controller, adjusts the current to apply the appropriate force based on the current position of the system and the reference value. The other system, the voltage-controller, controls the voltage in the electrical circuit in order to maintain the desired current, which is constantly changing due to the adjustments made by the first control system. This type of control system structure, known as a cascade PID, is shown in Fig. 2.3. It includes a faster inner loop and a slower outer loop, which control quantities that vary at different rates. The faster loop controls the faster changing states, while the slower loop controls the slower changing ones. In the context of this project, the faster changing quantity is the current and the slower changing quantity is the position, as determined by the discussion in Chap. 2.2. Laser sensor measurements from the four HEMS provide the feedback for this system. In this project, P_1 represents the transfer function of the magnet electrical circuit from voltage to current, and P_2 represents the EMS/HEMS system with the real current in the circuit as the input and the levitation air-gap as the output. The input to C_1 will be the difference between the reference air-gap and the actual one, while the input to C_2 will be the difference between the needed current and the actual current in the circuit.

Now that the necessary theoretical background has been established, it is possible to move on to the implementation of a control system to solve the levitation problem. In order to conduct a simulation, the geometrical and physical parameters of the two levitation systems must be determined. This allows to design the control system architecture in a way that is appropriate for the specific problem at hand.

Chapter 3

Methods

In this chapter, the methodology used to design a controller for the levitation of the pod is presented. The main focus of the work is to carefully analyze the characteristics of the system and make informed decisions about how to develop a mathematical model that accurately represents it. Modeling of the system requires multiple iterative phases, during which the model is continually refined and improved. The controller is then designed based on the insights gained from the analytical model.

In this study, the modeling of the system is divided into two parts: vertical levitation and lateral guidance. These two aspects of the system are equally important for the overall performance of the pod, and therefore require separate attention in the modeling process. In the following sections, a detailed overview of the steps taken to design the controller is provided, including the considerations made about the system, the process of modeling the system, and the design of the controller itself.

3.1 General Modelling Approach

In this section, the model developed for the levitation system is presented, along with an analysis of the key modeling decisions. The levitation pod is a six degree of freedom (DOF) system, which can be challenging to model and control. As a result, the system is divided into two subsystems: lateral guidance and vertical levitation. These subsystems operate independently, and the controller does not incorporate information from the other subsystem. The design and dimensioning of the HEMS/EMS system accounts for the independence of the systems assuring that, even in the case where all the electromagnets need the maximal current, the central power system is able to sustain the demand.

For vertical levitation, HEMS are used with four electromagnets placed below the rails that lift the entire weight of the pod. However, even a four point vertical levitation system still involves three rotations. To simplify the design further, the vertical levitation is split into four independent electromagnets, each carrying a quarter of the total mass of the pod and only allowed to displace vertically. As discussed in Chap. 2.2, this should not be a problem as long as the current rise time is significantly smaller than the dynamics time constant. Table 3.1 shows that in this case this condition is satisfied because the ratio r is less than one tenth, indicating that the current reacts more than ten times faster in the worst case scenario. Lateral stabilization for the pod is achieved using EMS, with four electromagnets placed inside the rails facing outward, two in the front and two in the back. To simplify the model for this direction, the control is split between the front

and back electromagnets. These electromagnets are only able to displace horizontally and are operated using a heuristic strategy, in which only one coil is used at a time to stabilize lateral movement. This strategy will be further explained in Chap. 3.3.3.

The objective of this project is to effectively evaluate the effectiveness of levitation systems. The selected model streamlines the analysis by breaking down the 6 degrees of freedom (DOF) of the pod into separate bodies with 1-DOF each (HEMS/EMS). It is therefore necessary to check whether it is possible to simplify the system without neglecting possible dangerous rotation of the 6-DOF system that could lead to instabilities due to the virtual shift of the center of gravity. It is therefore necessary to determine the magnitude of the maximal allowed inclinations in all the rotation directions.

Given the maximal displacement of the vertical control system at 1 cm and the maximal displacement of the lateral movement at 3 mm, the worst case scenario would result in a difference at the ends of the pod center-lines of 2 cm in both the y- and x-axis directions, and a difference of 6 mm with respect to the z-axis. The pod has a length of $l = 2.3\,\mathrm{m}$ and a width of $w = 0.9\,\mathrm{m}$, which translates to pitch angles of $0.5°$ for the x-axis, $1.28°$ for the y-axis and $0.15°$ for the z-axis. The maximum inclination of the pod can be calculated by considering the displacement as limited. This assumption is supported by the fact that, in reality, the pod is equipped with rigid wheels that act as hard stops and prevent excessive displacement. As a result, it is possible to accurately determine the maximum misalignment, that, even in the worst case scenario, produce small pitch and rotation angles.

3.1.1 Sensors Placement

In order to model the system accurately, it is important to properly center the pod. This is achieved using twelve distance sensors and the guidance levitation system. The sensors are divided into a group of six for the front and six for the back, and provide information for the control algorithm. The two sensors in the middle of the pod on either side of the middle toothed rail are used to measure misalignment with respect to the center line. The goal of the lateral guidance is to keep the pod perfectly centered with respect to the center rail, such that the propulsion motor is in the ideal position with respect to the center rail. This is necessary because even small differences in these gaps can produce a strong disturbance force caused by the motor. Two other sensors are placed

Table 3.1: Time constants for the electrical circuit and dynamics calculated analytically using eqs. (2.10) and (2.11), as well as the ratio between them. Given that the ratio is small, this allows to model each EMS/HEMS independently, thus simplifying the modelling of the system.

Parameter		**Value**
Current rise time	$t_{\mathrm{delay,el}}$	$1.135\,\mathrm{m\,sec}$
Dynamic time constant	$t_{\mathrm{delay,dyn}}$	$15\,\mathrm{m\,sec}$
ratio	r_{delay}	0.075

on the sides of the pod facing the L-shaped rails and are used to measure the distance between the lateral EMS and the rails. This distance measurement enables the control algorithm to compensate for potential disturbances in the shape of the rails, such as not perfectly straight rails or misalignment at conjunctions. Ideally, following (2.8), when there is a disturbance in the rail shape, for example bending, the air gap increases and the electromagnetic force decreases. It is important to note that the disturbance force has not changed with the bending because it is only dependent on the central misalignment. Therefore the controller is only compensating the force lost by the increase in the air gap by increasing the current. The four measurement are meant to work together to keep the pod centered. Finally the last two sensor are placed on the side of the of the pod facing upwards and measure the distance between the top of the rail and the HEMS. This information is used by the current-controller of the vertical levitation system to levitate the pod vertically.

3.1.2 Electrical Circuit

For a complete modelling of the levitation systems, one should also model the electrical circuit responsible for delivering the current to the electromagnets coil.

As shown in eqs. (2.6) and (2.8), the electromagnetic force applied by the electromagnet only depends on two variables: air gap distance and current. The air gap distance, both lateral and vertical, can be recovered by integrating twice (3.8) and (3.15) with respect to the time, whereas the current cannot be controlled directly and need to be calculated using the electric circuit dynamics. This comprises the voltage supplier, the resistance of the coil and the inductance produced by the electromagnet winding. The circuit is ideally coupled together by

$$\begin{aligned} U(t) &= RI(t) + \frac{\partial(L(t)I(t))}{\partial t} \\ &= RI(t) + \frac{\mu_0 N^2 A}{2}\frac{\dot{I}(t)}{\delta(t)} - \frac{\mu_0 N^2 A}{2}\frac{I(t)\dot{\delta}(t)}{\delta(t)^2} \end{aligned} \tag{3.1}$$

where $U(t)$ is the voltage of the electrical circuit, $I(t)$ is the current in the circuit, $L(t)$ is the inductance of the coil and $R(t)$ is the resistance, which is calculated using

$$R = \rho\frac{l_\mathrm{w}}{A_\mathrm{w}} \tag{3.2}$$

where l_w is the length of the coil and A_w is its cross section. It is assumed that the rise time of the current is much smaller than the dynamics' time constant. This decision, better explained in sec. 2.2, allows to assume that the current is able to change much faster than the pod moves. This assumption is validated by the values in Tab. 3.1.

Therefore, if a small enough time interval is considered, it can be assumed that the air

gap distance is approximately constant and therefore also the inductance expressed by

$$L = \frac{\mu_0 N^2 A}{2\delta(t)} \tag{3.3}$$

where A is the air-gap cross section, is assumed to be constant over the time interval. This allows to set the derivative of the inductance to zero in (3.1), which then becomes

$$U(t) = RI(t) + \frac{\mu_0 N^2 A}{2} \frac{\dot{I}(t)}{\delta}. \tag{3.4}$$

When considering the chosen control loop structure depicted in Fig. 2.3, the voltage control loop is the inner loop, and, thanks to the previous assumption, it is assumed that all quantities related to the outer loop are constants. This allows to model it in the same form as (3.4). When the Laplace transform is applied to this equation, it becomes

$$U(s) = RI(s) + sLI(s) \tag{3.5}$$

where R is the resistance and L is the inductance. This equation can be rewritten as

$$I(s) = \frac{1}{R + sL} U(s) \tag{3.6}$$

thus obtaining the transfer function from the voltage to the current

$$P_1(s) = \frac{1}{R + sL}. \tag{3.7}$$

It is important to note that the allowed current range for each of the pod subsystems is determined a priori by the Swissloop mechatronics team, and it's based on the capacity of the central unit to deliver current to all subsystems as well as on an estimation on the current needed to run that particular task. In the specific case of the EMS/HEMS, the estimation entailed a thermodynamic analysis to determine the corresponding heat dissipation.

3.2 Vertical Levitation Model

This section provides a detailed description of the vertical levitation system, including the geometry of the system and the general model of the HEMS. It also introduces the control system. The steps leading to the final mathematical model are also outlined.

3.2.1 System Dynamics

For the vertical levitation system, the first step is to model the dynamics of the system, shown in Fig. 3.1, using Newton's second law of motion and assuming no change in the mass of the system m. Then the equation governing the dynamics of the system is given

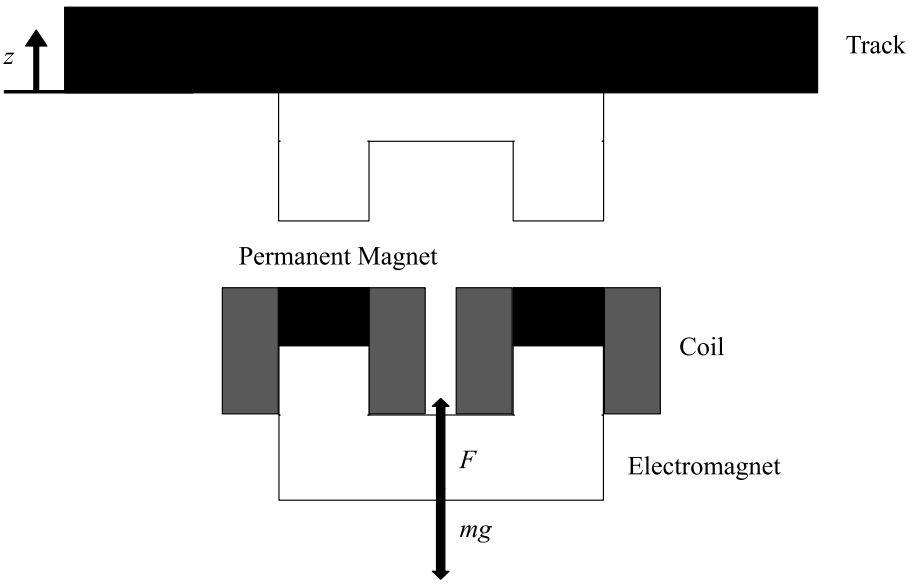

Fig. 3.1: Sketch of the general concept of magnetic levitation system obtained combining a permanent magnet (black), with an electromagnets that uses coils (grey) with flowing current to generate a magnetic field. The magnet is used to counteract the weight force of the vehicle and its inertia. The force F represents the electromagnetic force and it is modelled using (2.6).

by

$$m\frac{d^2z}{dt^2} = F_{\text{HEMS}} - F_g = F_{\text{HEMS}} - m \cdot g \tag{3.8}$$

where z is the air gap between the levitating rail and the electromagnet's ends, m is the total mass of the considered system, g is the gravitational constant and F_{HEMS} is the electromagnetic force produced by the electromagnet according to (2.6). It is clear from (3.8) that the system of reference is facing upwards, so that a large negative z means that the pod is falling down.

3.2.2 Geometrical considerations

The geometry of the EMS is significant in determining the mass of the system and the mechanical force, which depends on the air gap cross section, as can be seen from eqs. (2.3) and (3.8). The air gap cross section is calculated using

$$A_{\text{core}} = w_{\text{core}} \cdot d_{\text{core}}. \tag{3.9}$$

To determine the mass of each HEMS, it is necessary to know the amount of coil mass required in addition to the number of windings, core geometry and weight of the

permanent magnets. To calculate this quantity, an approximation of the thickness of the coil when wrapped around the core must first be made. This thickness, referred to as h_c, is calculated using

$$h_c = d_{\mathrm{w}} \cdot \frac{d_{\mathrm{w}} \cdot N_{\mathrm{c}}}{l_{\mathrm{core}}} \tag{3.10}$$

where d_{w} is the coil diameter, N_{c} is the number of winding and l_{core} is double the length of the electromagnet's arms. then it is possible to approximate the needed coil mass as

$$m_{\mathrm{c}} = ((2 \cdot h_{\mathrm{c}} + w_{\mathrm{core}}) \cdot (d_{\mathrm{core}} + 2 \cdot h_{\mathrm{c}}) - w_{\mathrm{core}} \cdot d_{\mathrm{core}}) \cdot l_{\mathrm{core}} \cdot \rho_{\mathrm{Cu}} \tag{3.11}$$

where w_{core} is the core width, d_{core} is the depth of the core and ρ_{Cu} is the density of the copper used for the coil. At this point, it is easy to find the mass of the single HEMS

$$m_{\mathrm{HEMS}} = m_{\mathrm{c}} + m_{\mathrm{perm,mag}} + (l_{\mathrm{core}} + 2 \cdot w_{\mathrm{core}} + 4 \cdot h_{\mathrm{c}}) \cdot A_{\mathrm{core}} \cdot \rho_{\mathrm{Fe}} \tag{3.12}$$

There are four HEMS for the levitation system, therefore the total mass of the system is given by

$$m_{\mathrm{total}} = m_{\mathrm{p}} + 4 \cdot m_{\mathrm{HEMS}} + 4 \cdot m_{\mathrm{EMS}} \tag{3.13}$$

where m_{p} is the mass of the the pod without the EMS and the HEMS and m_{EMS} is the mass of the EMS according to (3.12) without accounting for the weight of permanent magnets. This quantity represents the upper limit for the weight of the pod set during the objective definition phase of this year Swissloop pod. This value is used as a worst case scenario given that the pod is not built yet. Additionally, as can be seen in (2.3), the mechanical force produced is directly proportional to the air-gap cross section, which is equal to the electromagnet cross section as no fringing or leakage is assumed [13]. It is worth noting that the cross section expressed in equation (3.9) is a key optimization parameter because, on one hand, it increases the applied force, but on the other hand, it also increases the mass of the system and therefore the weight force acting in opposition to levitation.
To address the cross section optimization problem, it is necessary to first determine the bounds of this surface based on the different possible configurations of the system and their characteristics.

3.2.3 Orientation of the Electromagnets

One of the main considerations in designing the electromagnets includes the decision on the best orientation. Referring to Fig. 3.2, the two options are aligning the axis of the pod's forward either in parallel with the longitudinal axis of the electromagnets or perpendicularly . The perpendicular option, shown in Fig. 3.2(b), has been used successfully by companies working on Hyperloop concepts, such as HARDT [15], but still has some challenges in terms of force generation. On one hand, the size of the electromagnet would be limited by the width of the rail, limiting the generated force,

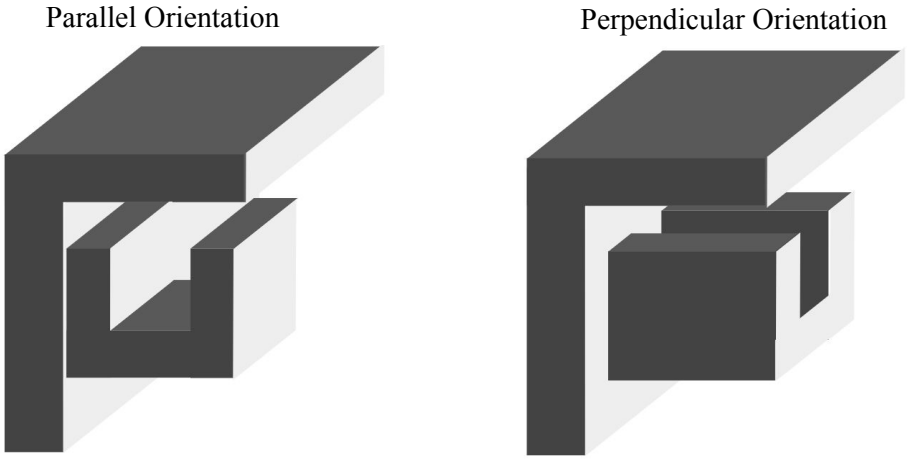

(a) (b)

Fig. 3.2: Two different options for the orientation of the HEMS/EMS system.

which is proportional to the air gap cross section. One solution could be to use multiple electromagnets in series for this orientation, but this would make control more complex. Another option to increase the applied force is to widen the u-shaped core, increasing the cross section. However, this would also require increasing the space between the two arms of the u-shape to accommodate the wrapped coil, resulting in a very wide u-shape and a longer path for the flux loop to close, leading to core losses and losses due to fringing and leakage. An optimal u-shaped magnet would have the two poles close together to facilitate the closure of the magnetic field loop.
After comparing both options, the results shows that aligning the axis of the pod's forward movement with the y-axis (as shown in Fig. 3.2(b)) has undesirable behavior at high speeds. This is demonstrated in Fig. 3.3, which plots the generated force versus traveling speed. Higher speeds results in a significant drop in the generated force compared to the static case, as seen in simulations at five different speeds for a range of air gaps. Upon further analysis, at high speeds, the electromagnet does not have enough time to change the magnetization state of the track, causing the magnetic flux to close over a longer path and creating magnetic drag. This can be seen in Fig. 3.4, which show the magnetic flux loop for various speeds. At zero speed the loop closes nicely over the air gap and the track material is magnetized in a concentrated area. However, as the speed increases, the closure of the magnetic loop appears to be dragged along with the movement of the magnet. One possible explanation for this is that as the right side of the magnet magnetizes the material in one direction (e.g. counterclockwise), when it passes the area where the right side was, tries to pull the flux in the opposite direction. This can be thought of as two tangent circles with the same turning direction that have opposite directions of motion at the point of contact. Additionally, as the magnet is moving, it is not able to reconstruct the flux loop at each step due to the time required

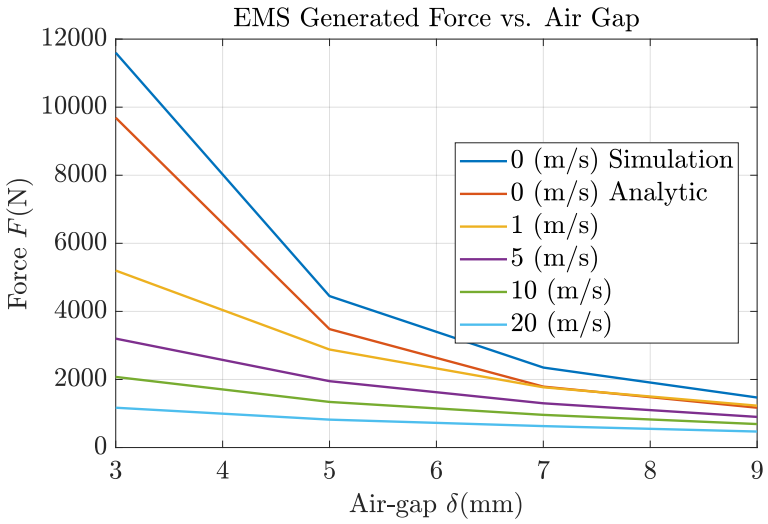

Fig. 3.3: Graph showing the dependencies between generated force and speed for the perpendicular orientation on Fig. 3.2. It clear from this graph that the speed as a significant effect on the generated force for this electromagnet orientation. For an air gap of 6 mm the generated force decrease of more than 3000 N from the static case to the maximal speed case, making it impossible to compensate the weight of the pod. This graph also shows the validity of the developed analytical model that presents similar results to simulation ones.

for magnetization, leading to the drop in generated force at higher speeds.

The second orientation option is shown in Fig. 3.2(a). This configuration has two main advantages. First, it allows for an increase in the applied force by increasing the air gap cross section without increasing the number of windings, as the depth of the electromagnet is no longer limited by the size of the track. The second advantage is that there is no need to reconstruct the magnetic field loop at each step as the material will always be magnetized in the same direction. It is clear that this latter orientation is more suitable for the application, and is therefore chosen as the configuration for both the HEMS and EMS. This choice is further supported by preliminary simulations, the results of which are shown in Fig. 3.6. In this graph, it can be seen that the effects of speed on the generated force are less strong compared to the results for the perpendicular orientation.

Fig. 3.5 shows the final design of the HEMS system, which demonstrates the application of the insights gained from this analysis. The design consists of a deep electromagnet with the purpose of increasing the active air gap cross section and thus the generated force.

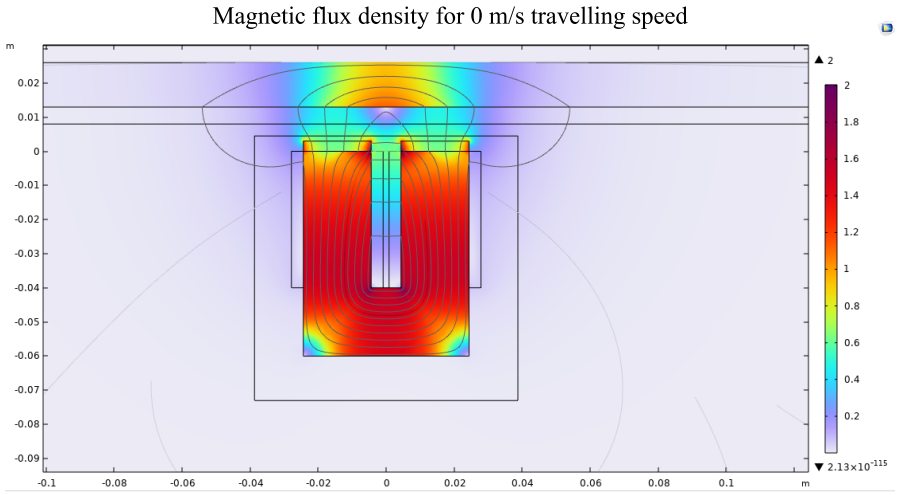

(a)

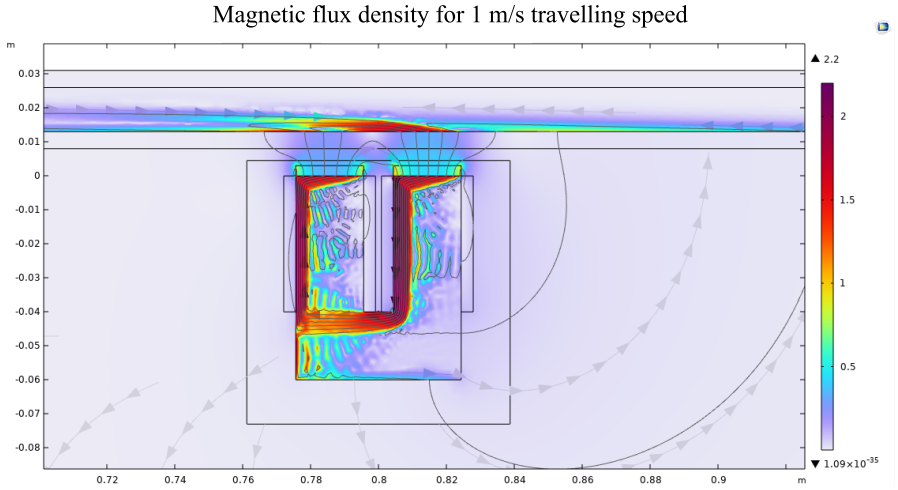

(b)

Fig. 3.4: Fig. 3.4(a) shows the magnetic flux loop for the static case, while Fig. 3.4(b) shows the magnetic flux loop for 1 m s^{-1} travelling speed. For this simulations the direction of the travelling speed is pointing to the right. From this simulations it possible see what causes the force drop in Fig. 3.3 for increasing speeds. It is in fact clear that, as the speed increases, the electromagnet is not able to magnetize the material of the track around the electromagnet fast enough, and the magnetic flux loop appears to be dragged along with the movement, thus weakening the magnetic field in the air gap and, consequently, the generated force.

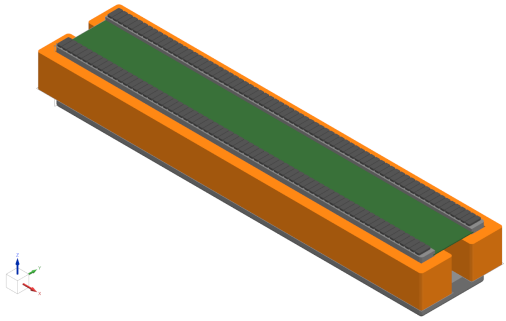

Fig. 3.5: This figure shows the final 3-D model of one HEMS. The orange component represents the coils, the grey part is the core of the electromagnet and the black pieces on the top are the permanent magnet. The presence of permanent magnets is the only difference with respect to the 3-D model of the EMS.

3.2.4 Adding Permanent Magnets

The use of permanent magnets in addition to electromagnets is implemented in the system design to minimize current usage, thus reducing the energy usage and the workload on the central management system. The employment of strong permanent magnets allows for the possibility of reducing the electromagnetic force to near zero through the application of negative current, as depicted in Fig. 3.6. This is beneficial in the event that the pod is too close to the rails. It is also demonstrated in Fig. 3.6 that applying a current of zero results in the force being produced solely by the permanent magnets, representing an ideal operating point of minimal power consumption while maintaining stability. Therefore, the main purpose of permanent magnets is to compensate as much as possible the DC offset of the weight of the pod, while that of the electromagnet is to handle changes in reference and possible disturbances in the track, i.e. misalignment at the junctions. The objective of the control system should therefore be to operate as close to a current of zero as possible while ensuring stability.

3.2.5 Control system - vertical levitation

The control loop for the vertical levitation can be established once the system's geometric parameters and configuration have been determined. Fig. 3.7 illustrates the general structure of the control system, including all relevant components and subsystems. The outer-loop PID controller, located in the top left of Fig. 3.7, outputs the required current based on the difference between the current air gap and the reference distance. This controller is chosen for its versatility and ease of tuning, and includes saturation and anti-windup features to limit its output. The saturation prevents the controller from

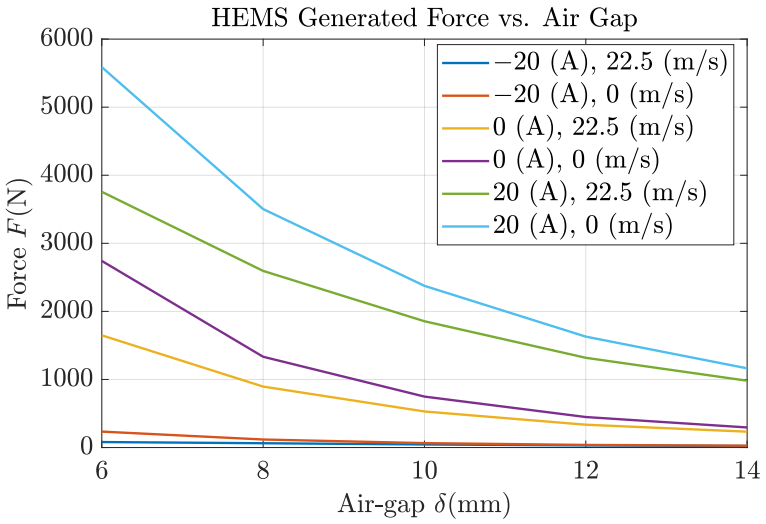

Fig. 3.6: Simulations for the generated electromagnetic force as a function of current, air gap and travelling speed. For this simulation the parallel orientation of Fig. 3.2 is chosen. From this graph, the differences with Fig. 3.3 are clear. Using this orientation, the effects of the speed on the force generation are limited, allowing the magnet to produce enough force to levitate also at high speed.

exceeding limits on the current that the central unit can allocate to each subsystem, avoiding overload on the central unit. The electrical circuit subsystem is located on the right of the controller. As shown in Fig. 3.8, this subsystem constitutes the inner-loop of the cascaded PID controller structure chosen for the project and enables regulation of the current output while considering the dynamics of the electrical circuit. The dynamics of the electrical circuit must be accounted for due to the inductance of the coil, which causes a delay in the actual current output. The PID controller located in the top left of Fig. 3.8 regulates the voltage applied to the circuit and includes saturation and anti-windup elements for the previously mentioned reasons. The block adjacent to the controller represents the transfer function from voltage to current according to (3.7). The inductance subsystem, depicted in Fig. 3.8, calculates the inductance of the system at each time step. It is important to continuously update the inductance value as it depends on the air gap, a time-varying state of the system, according to (3.3). Finally, the output of the transfer function, which represents the actual current present in the circuit, is again limited based on the range in Tab. 3.2. The three-dimensional look-up table in Fig. 3.7 translates the applied current to the generated force, taking into account the current air gap and traveling speed of the pod. Alternatively, the mathematical model represented in (2.6) could be utilized, but this approach has limitations as it cannot account for the traveling speed and the behavior of the permanent magnet may be nonlinear due to hysteresis losses. Therefore, simulations are performed for various combinations of

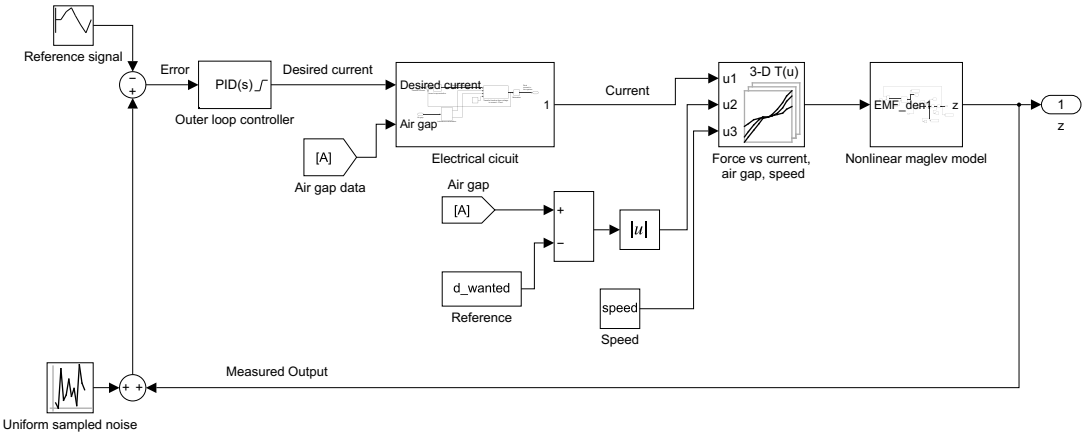

Fig. 3.7: This figure shows the Simulink model for the HEMS system. In this model all the fundamental components of the cascaded structure are visible. The outer loop is made up of the outer control loop and the non linear maglev model, while the electrical circuit block represents the inner loop. This block is expanded in Fig.3.8. The outer loop controller regulates the current based on the difference between the current air gap and the desired one. In this figure it also visible the 3-D look up table that expresses the force generated by the HEMS as a function of the current, air gap and speed of the pod.

current, speed, and air gap using ANSYS software, the results of which are shown in Fig. 3.9. The SIMULINK 3-D look-up table also allows for interpolation between data points, enabling accurate simulation of the system's behavior. A cubic-spline interpolation is used instead of linear interpolation due to the convex behavior of the electromagnetic force as a function of the inputs. Linear interpolation between data points could potentially overestimate the generated force for certain input combinations.
Finally the nonlinear maglev model block in Fig. 3.7 simulates the nonlinear dynamics of the levitation system described in (3.8). This subsystem takes the HEMS force as input and produces the current position as output, which is obtained by isolating the acceleration in (3.8) and integrating it twice. It is important to note that an additional force is introduced in (3.8) coming from the aerodynamic lift, F_{L}, which is applicable for planned tests in atmosphere instead of the vacuum tubes, which do not exists for this application yet. Then (3.8) becomes

$$m\frac{d^2x}{dt^2} = F_{\mathrm{HEMS}} + F_{\mathrm{L}} - F_g. \tag{3.14}$$

This force is calculated to be in the order of 180 N at the top speed of $22.5\,\mathrm{m\,s^{-1}}$ and 0 N when the pod is still.

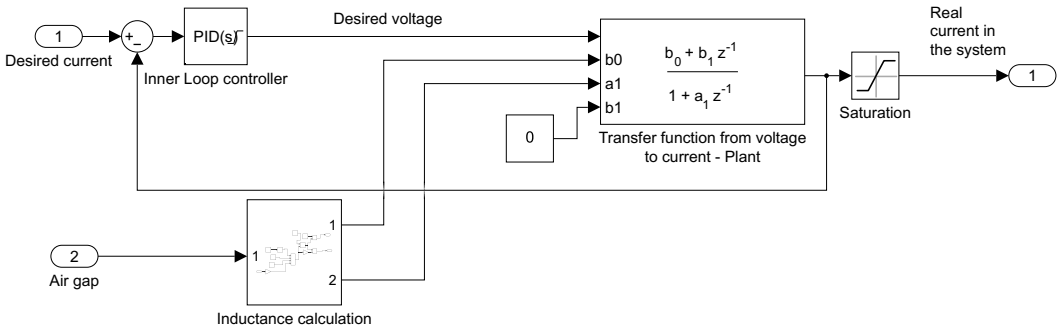

Fig. 3.8: Inner control loop for the electrical circuit of the HEMS/EMS electromagnet. The PID controller regulates the voltage of the circuit and includes saturation and anti-windup elements. The block adjacent to the controller represents the transfer function from voltage to current according to (3.7). The dynamic block on the bottom calculates the inductance at every time step according to (3.3).

3.3 Lateral Guidance Model

This section discusses the lateral guidance system. The system has many similarities to the HEMS system, so the focus lies on the operational strategy, motor disturbance force, and generated force. The relevant parameters for the EMS system are shown in Tab. 3.3.

3.3.1 System Dynamics

In the case of the lateral stabilization, the dynamic of the system is the following

$$m\frac{d^2y}{dt^2} = F_{\text{EMS}} + F_{\text{d}} \tag{3.15}$$

where F_{EMS} is the force generated by the EMS according to (2.8) and F_{d} is a varying disturbance force, which comes from the reluctance motor. As already discussed in Chap. 1, the new reluctance motor employed on the Swissloop pod, does not allow for passive lateral stabilization anymore. As long as the motor left and right sides are perfectly aligned with the track teeth in the center, the resulting lateral force component is zero. But if there is a misalignment, e.g. the motor left coil is closer to the teeth than the right one, there will be a resulting lateral force pulling the pod towards the teeth, i.e. $\frac{dF_{\text{d}}}{dt} > 0$. For explanation sakes, assume that also the reluctance motor force can be approximated through (2.8). Also assume that the left and right electromagnets of the motor are the same, i.e. same number of winding, same current, and same cross section. Then, F_{d} can

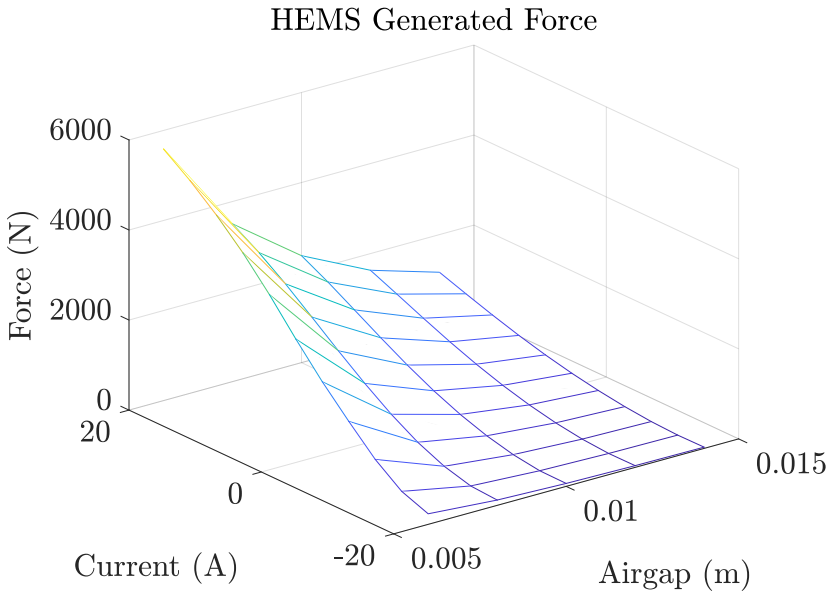

Fig. 3.9: This figure shows the force generated by each HEMS as a function of three inputs: current, air gap, and speed. The results shown in this plot are for the speed of $0\,\mathrm{m\,s^{-1}}$. This graph, together with the corresponding ones for $5\,\mathrm{m\,s^{-1}}$ and $22.5\,\mathrm{m\,s^{-1}}$ travelling speed, constitute the 3-D look-up table used in the Simulink model of Fig. 3.7. An important feature of this table is that the generated force is at the minimum when the current is at $-20\,\mathrm{A}$, meaning that the electromagnet is able to fully counteract the field generated by the permanent magnet.

be approximated to

$$F_\mathrm{d} = \frac{(NI)^2 A\mu_0}{4\delta_\mathrm{l}^2} - \frac{(NI)^2 A\mu_0}{4(\delta_\mathrm{eq} - \delta_\mathrm{l})^2} \tag{3.16}$$

At this point it is clear that if the left coil is closer to the teeth, i.e. $\delta_l < \delta_\mathrm{eq} - \delta_\mathrm{l}$, then F_d will be positive and, given that it is only possible attract with electromagnets, the pod will be pulled to the right towards the teeth.

To better model the disturbance force, simulations are conducted on the motor to accurately determine the generated force as a function of speed, misalignment, and applied current. Fig. 3.10 shows the results of simulations for the resulting lateral component of the disturbance force. A notable characteristic of the motor force is the presence of ripples in the force profile. These ripples are caused by the air gap-dependent change in reluctance within a phase. At the beginning of the phase, there is minimal overlap between the motor and the tooth, resulting in a low propelling force. As the pod advances, the overlap increases, leading to an increase in the generated force. One

annotation is that these ripples are bad for lateral guidance but not for overall propulsion because higher ripple translates to higher propelling force.

For simulation purposes, only the highest absolute value of these ripples is considered. Two significant trends can be observed in Fig. 3.10. The disturbance force decreases as the speed increases, and the force ripples flatten out with increasing speed. These effects can be attributed to the skin effect, in which the volume through which the magnetic field flows decreases as the frequency (related to the traveling speed) increases, leading to a decrease in the magnetic flux and resulting force.

3.3.2 Geometrical considerations

The fundamental concept behind the EMS is similar to that of the HEMS, including the shape of the electromagnets and their orientation. However, as shown in Tab. 3.3, there are some differences in the intrinsic parameters, such as the number of windings, current range, width of the u-shaped profile, and diameter of the coil. These changes, as well as the decision to not use permanent magnets in the EMS system, are made to optimize the system for its intended use and operational strategy. Some parameters are adjusted due to the higher forces required to counter the motor disturbance force, which is significantly stronger than the weight force of the pod.

The decision to not use permanent magnets in conjunction with the EMS system is made to increase energy efficiency. In the case of vertical levitation, efforts are made to use as little current as possible to levitate the pod, so sufficient permanent magnets are used to levitate around a chosen air gap without requiring any additional force. The use of permanent magnets in this case is dictated by the constant downward force of the pod's weight.

In the case of lateral guidance, if the misalignment is zero, the lateral component of the propelling force of the right coil is equal to that of the left coil, resulting in a total force of zero and no current requirement to maintain this position. However, in the case of misalignment, one side of the motor will have a smaller air gap and generate more force for the same current, as shown in (3.16). Additionally, the resultant force from the misalignment of the permanent magnets on the two opposing EMS systems, as described in (3.16), would further complicate control of the lateral movement due to the increased forces involved.

Therefore, the ideal situation would be to generate a force in the opposite direction of the disturbance force. This consideration led to the development of the control strategy for lateral guidance.

3.3.3 Operational strategy for the lateral guidance

To maximize the energy efficiency in the lateral guidance system and minimize misalignment, it is decided to operate the EMS in pairs, with one pair for the front and one for the back, and to only operate one EMS at a time within each pair. This approach is adopted for two reasons: to avoid using MIMO (multiple input, multiple output) systems and to avoid adding additional forces in the direction of the disturbance force.

Operating only one EMS at a time allows the use of conventional controller designs, similar to those used for vertical levitation, to generate forces in both lateral directions.

Additionally, operating both EMS at the same time carries the risk of introducing more force in the direction of the disturbance force due to the difficulties of precisely controlling a MIMO system. For example, if the misalignment is to the left and the resulting disturbance force is also to the left, the left EMS will continue to produce a force to the left as long as it has current flowing. The right coil would then need to increase its current even further to compensate for the force still being generated by the left side.

To address this issue, it is decided to only operate one EMS at a time by checking the direction of the misalignment and completely shutting off the other EMS. In the simulations it is assumed that the current in the EMS goes to zero immediately when switched off.

3.3.4 Simulink model for the Lateral Guidance

This section presents the Simulink model for the lateral guidance system, with a focus on the differences between this model and the vertical levitation model. The control loop structure remains unchanged, but there are two main differences in the EMS look-up process. First, there is an additional look-up table to calculate disturbance forces. Second, the inputs to the EMS look-up table are the current, the traveling speed, and the difference between the currently measured distance and the equilibrium position. Fig. 3.11 shows the section of the Simulink model responsible for calculating the force generated by the EMS. A look-up table is used instead of a mathematical model due to its higher accuracy in representing the produced force. For simulation purposes, the system is assumed to be rigid and the rails to be completely straight. This allows the calculation of all four distance measurements without the need to simulate four independent sensor measurements. The starting equilibrium positions are a 5 mm air gap between the teeth and the motor coil and a 5 mm gap between the rails and the EMS. Only one measurement is taken, in this case the distance between the left EMS and the rail. From this measurement, it is possible to calculate the other air gaps at each time step by knowing the difference between the left air gap and its original equilibrium position. This delta calculation is important as it determines which EMS should be active based on the convention

- $\Delta < 0 \rightarrow$ Right EMS on, left EMS off
- $\Delta > 0 \rightarrow$ Right EMS off, left EMS on
- $\Delta = 0 \rightarrow$ Right EMS off, left EMS off

The active EMS is simulated by changing the sign of the current. Although the current in the EMS can only take positive values in the range $0 - 20$A, for the simulations, a negative current indicates that the right EMS is active. Fig. 3.12 shows the force profile generated by the EMS as a function of the applied current and the air gap. It is important to note that the higher the air gap, the lower the generated force, as expected.

To assess the suitability of the controller for practical application for both systems, it is necessary to discretize the control system and simulate the response in order to compare the performance of the continuous and discrete systems. The discretization will be addressed in the next section.

3.4 Discrete control system

Discretizing the system on SIMULINK is straightforward. It is only necessary to substitute all the blocks with the discrete version. The sampling frequency is set to the measurement frequency of the distance sensor and is equal to $f_{sampling} = 2\,\text{kHz}$. Although the transitioning is straightforward, some blocks need some adjustment during the transition. One is the transfer function from the voltage to the current used in the inner control loop. The approach is to discretize it using the Euler backward method

$$s = \frac{z - 1}{z \cdot T_{sampling}}. \tag{3.17}$$

Using this discretization approach, the controller manages to stabilize the system and follow the reference value. Contrary to the forward case, the Euler backward discretization method usually preserves the stability for asymptotically stable continuous-time system [16].

Table 3.2: Relevant parameters for modelling the vertical levitation system.

Parameter		**Value**
Number of windings	N_c	230
Core width	w_{core}	17 mm
Core length	l_{core}	64 mm
Core depth	d_{core}	42 cm
Coil diameter	d_{coil}	1.2 mm
Max. Current	$I_{c,max}$	20 A
Min. Current	$I_{c,min}$	−20 A
Pod mass	m_{pod}	180 kg
Coil cross section	A_{coil}	0.7854 mm^2
Core cross section	A_{core}	1 cm^2
Coil height	h_c	20 mm
Coil mass	m_{coil}	2 kg
HEMS mass	m_{HEMS}	7.93 kg
Total mass	M_{total}	237 kg

Table 3.3: Relevant parameters for modelling the lateral guidance system

Parameter		**Value**
Number of windings	N_c	380
Core width	w_{core}	17 mm
Core length	l_{core}	72 mm
Core depth	d_{core}	30 cm
Coil diameter	d_{coil}	1 mm
Max. Current	$I_{c,max}$	20 A
Min. Current	$I_{c,min}$	0 A
Pod mass	m_{pod}	180 kg
Coil cross section	A_{coil}	0.82 mm^2
Core cross section	A_{core}	51 cm^2
Coil height	h_c	20 mm
Coil mass	m_{coil}	1.86 kg
EMS mass	m_{EMS}	6.35 kg
Total mass	M_{total}	237 kg

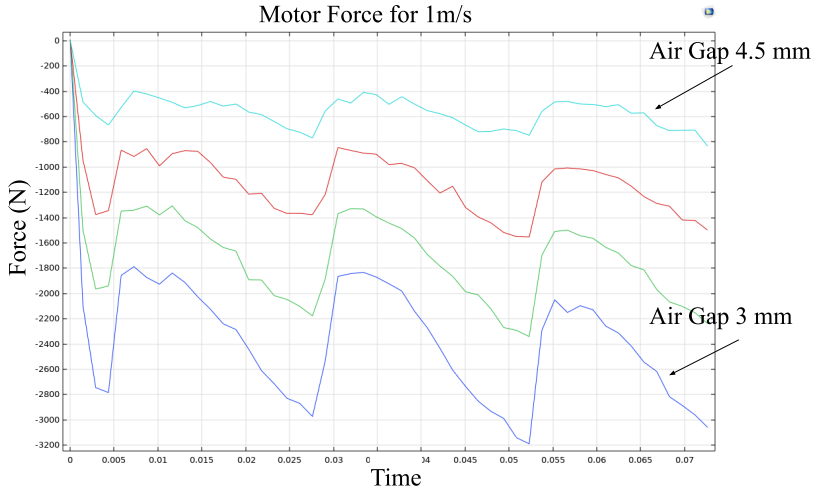

(a)

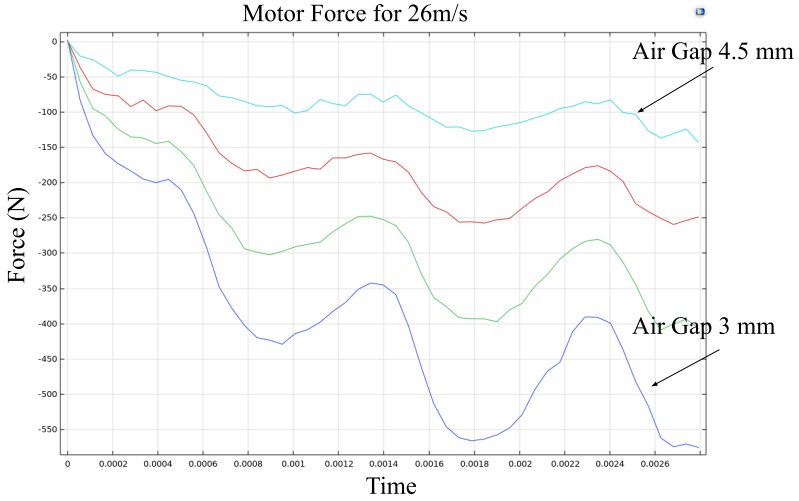

(b)

Fig. 3.10: Results of the simulations for the lateral component of the propulsion force as a function of the travelling speed and air-gap distance. Fig. 3.10(a) shows the simulation for a travelling speed of $1\,\mathrm{m\,s^{-1}}$ and Fig. 3.10(b) for $21\,\mathrm{m\,s^{-1}}$. It is possible to note that the ripples oscillates over a wider range for lower speeds, and in general the generated force is lower for high speed. This is because the time interval in which the motor coil overlap with a track teeth decrease as the speed increases, and the motor has less time to magnetize the track, thus generating less propulsion force. The two graphs only show the negative side of the lateral force, where an air gap of 5 mm corresponds to the pod being perfectly aligned and zero lateral force. The positive side of the lateral force for the air gaps of 5-7 mm would mirrored around the 0 N-axis, given the symmetry of the system.

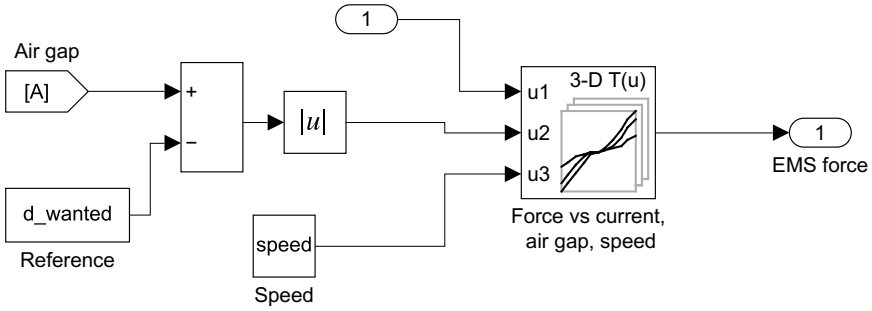

Fig. 3.11: This figure shows the look-up table that substitutes the numerical model for the EMS generated force. The look-up table inputs are the current, the air gap and the speed of the pod. The aig gap needs to be first converted to the difference with respect to the equilibrium position. This because if the air gap is less than the equilibrium point, the opposite EMS is activated to pull the pod towards the equilibrium point.

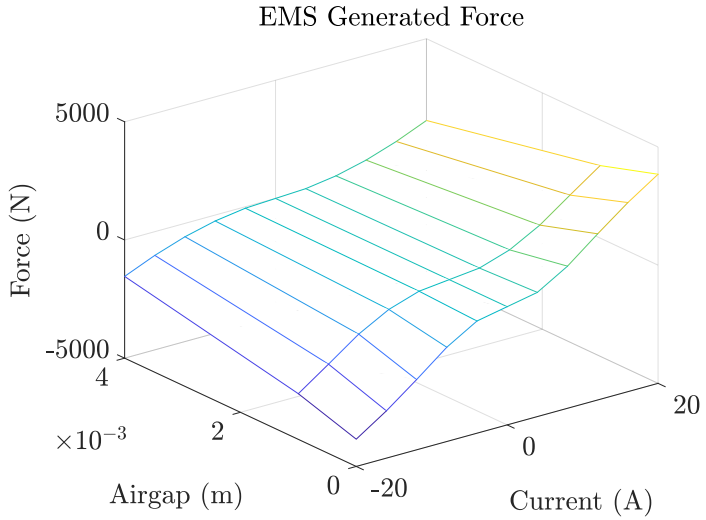

Fig. 3.12: Generated force as a function of the current and air gap for a travelling speed of $0.5\,\mathrm{m\,s^{-1}}$. Differently from Fig. 3.9, in this case the generated force is zero when the current is 0. The fact that the current is able to be both positive and negative represents a trick to simulate which EMS is active. When the controller outputs a positive current it means that the right EMS need to be active, while a negative current corresponds to the left EMS.

Chapter 4

Results

In this chapter, the results of the thesis are presented and discussed. The aim of the thesis is to investigate the performance of the proposed control system in maintaining the stability of the levitation system. The control system is implemented in SIMULINK and tested under various operating conditions. The results demonstrate the effectiveness of the control system in maintaining the stability of the levitation system and improving the tracking performance. The results are presented starting with the simulations of the lateral guidance and followed by the vertical levitation system. The results are analyzed and discussed in terms of the control performance and the effect of the various operating conditions on the levitation system. The main analyzed parameter are stability in terms of air-gap positioning, ability to track the reference value and acceleration of the pod. Finally, the main findings of the thesis are summarized and the implications for future work are discussed.

4.1 Reference Tracking

This section provides a more detailed explanation of the results obtained from running simulations on the guidance and levitation SIMULINK models, with a focus on the problem of tracking and following a changing reference.

The simulation results on the left of Fig. 4.1 are obtained by simulating the guidance system's ability to follow a changing reference air gap. This simulates a scenario where the reference air gap could be changed due to factors such as a bend in the rails or a misalignment at the rail junctions. By simulating this scenario, it is possible to evaluate the system's ability to maintain stability and continue travelling straight even when faced with these changing references.

The results obtained from the simulation without noise shows that the system behaves smoothly and is able to effectively track the reference, with a maximum overshoot of 0.5 mm. Additionally, the system is able to operate within the safe range of air gap without engaging the safety wheels. This indicates that the system is able to maintain stability and continue travelling straight even when faced with changing references.

However, when noise is added to the measurements, the system's performance is impacted. The noise added to the measurement is represented by an uniform number in the range -16-16 µm. This value is calculated based on the sensor information that assured the measurement error to stay below the 0.1% of the measured range. To be conservative, the measured range is assumed to always be 1 cm and an additional safety

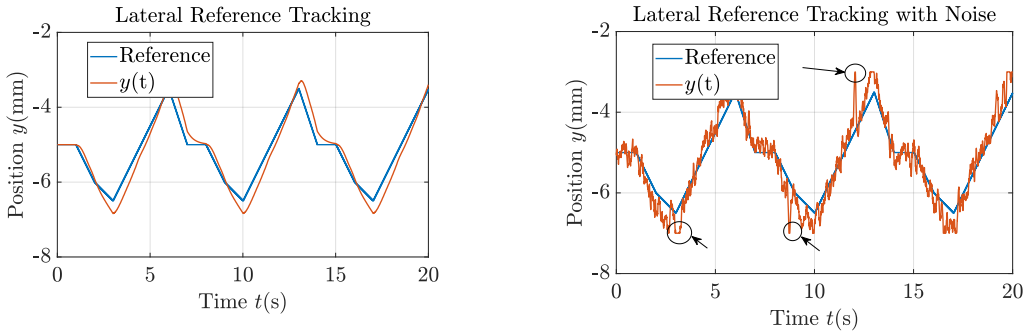

(a) (b)

Fig. 4.1: Results for the reference tracking of the lateral guidance system, which shows that the system is able to follow the reference well also when the measurement is corrupted with the noise. In this latter case, there are some instants in which the safety wheels are engaged, which is marked by the ovals and arrows. The noise applied to the sensor measurement is a uniform sampled number in the range -16-16 µm.

factor of 1.6 is applied. The system response is affected by the noise, resulting in an increase in overshoot and deviation from the reference. Additionally, the system is seen to operate at a wider range of air gap, which is evident in the engagement of the safety wheels at specific time points as highlighted in Fig.4.1(b).

In the case of the vertical levitation system, simulations are performed using a changing reference value that followed a series of positive and negative additive steps of various sizes. This type of reference is chosen to simulate the misalignment at the junctions between rail pieces. The results of the simulation are shown in Fig. 4.2 where the left graph illustrates the case without noise in the sensor measurement and the right graph shows the case with noise. For this simulation, the value of the noise is chosen to be uniformly distributed in the range -16-16 µm.

As observed in the graph representing the system without measurement noise, it is possible to see that the system is able to effectively follow the changing reference. The equilibrium point is set to 1 cm and the overshoot remains consistently below 1 mm. It is also notable the overshoot is more pronounced in cases where the reference goes below the equilibrium point. This can be attributed to the non-convexity of the generated force, which increases more rapidly for a smaller air-gap. Therefore, when the reference is smaller than the equilibrium point, meaning that the rail is closer to the electromagnet, the current has to change more to compensate for this non-convexity, leading to a higher delay.

The case with added noise in the measurement shows a different behavior. The system's performance is affected by the noise, resulting in increased overshoot and deviation from the reference. Nevertheless the system is able to remain withing the bounds of the allowed air-gap range 7-14mm. A clear deviation from reference is visible at 10 s on the right

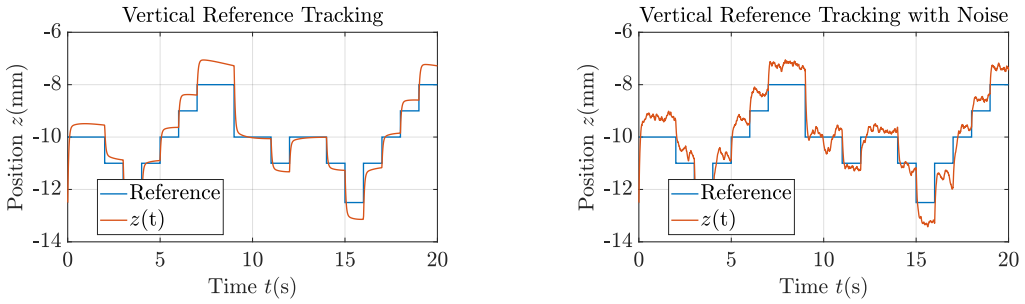

(a) (b)

Fig. 4.2: Results for the reference tracking of the vertical levitation system, which shows that the system is able to follow the reference well and to remain in the allowed air gap range also when the measurement is corrupted with the noise and the overshoot is more pronounced. The noise applied to the sensor measurement is a uniform sampled number in the range -16-16 µm.

graph of Fig. 4.2. The system's response became less accurate compared to the no-noise case.

It is important to note that the effect of the noise is more pronounced in the case of the lateral guidance with respect to the vertical levitation. The reason is that the noise applied to both systems is calculated based on the equilibrium position of the HEMS system which is double that of the EMS. Thus, there is an additional 1.5 safety factor, which compounded with the original safety factor of 1.6 makes up of a 2.4 safety factor overall for the lateral guidance system.

Overall, these results demonstrate that the proposed control system is effective in maintaining the stability of the levitation systems and tracking the reference within an acceptable range of air gap. Additionally, the simulation results show that the performance of the systems is significantly impacted by noise in the measurements and highlights the importance of accurate measurements and noise reduction in ensuring the stability, accuracy and safe operation of the system.

4.2 Acceleration

Right now the Hyperloop technology is only a prototype and the pod is not carrying any payload, but in the future this technology is meant to substitute conventional method of transport. Therefore an important parameter for the performance of the system is the acceleration that the pod undergoes, both lateral and vertical. The lateral acceleration of the pod is crucial for maintaining stability and ensuring the safety of the passengers or cargo. The vertical acceleration of the pod is important for the overall comfort and safety of the passengers or cargo during the transportation. High acceleration rates can cause discomfort and even injury to passengers or damage to cargo. Therefore, it is important to

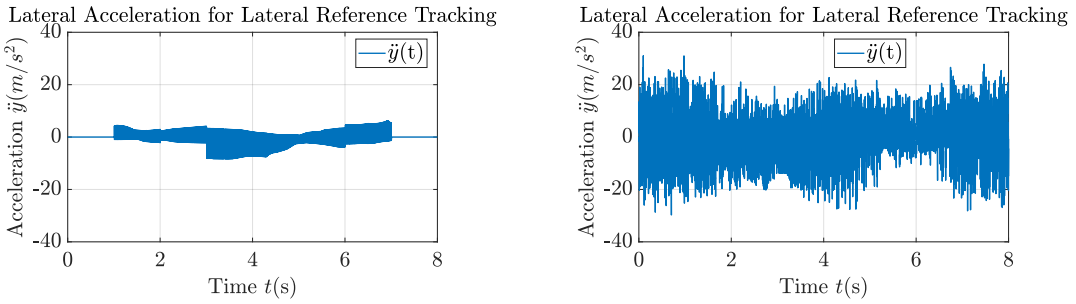

(a) (b)

Fig. 4.3: Results of the simulations for the acceleration in the guidance system subject to the changing reference air-gap of Fig. 4.1. The acceleration for the case without noise always remain contained in the $1G$ range, -9.81-9.81m s^{-2}, but when noise is applied to the sensor, the acceleration oscillates over a wider range of values.

carefully design and control the guidance and levitation systems to minimize acceleration rates while maintaining stability and safety of the pod. The resulting acceleration on the guidance system following the reference tracking of Fig. 4.1, is show in Fig. 4.3. The left graph represents the case without the noise, while the right graph has noise added to the sensor measurement. The situation with no noise presents accelerations bounded by $1G$ both on the positive and negative side.

However, when noise is added to the sensor measurement, right graph of Fig. 4.3, the results are different. The accelerations are higher and fluctuate more, reaching values of $3G$ at times. However, it is important to note that while the higher acceleration values are represented by spikes of a duration of hundredths of a second or even milliseconds, meaning that the derived displacement and speed are negligible if the spikes duration remains small. Nevertheless, it is important to consider that even if these acceleration are not a significant threat to the passengers, they could be dangerous for the structural integrity of the pod. Therefore, it is crucial to take these acceleration spikes into account when designing the structural components of the pod and testing its safety.

As can be seen in Fig. 4.4, the vertical acceleration results for the levitation system with and without noise are displayed. The results show that in both cases the accelerations remain mostly within the $1G$ interval. They tend to be lower compared to the lateral accelerations produced by the guidance system. This can be attributed to the fact that the forces involved in the lateral guidance are much higher than the ones that the electromagnets of the vertical system have to face.

Moreover, it is also important to take into account the vibration that this acceleration can produce, which can be perceived by the passengers as a discomfort. Therefore, it is important to design and tune the control system to reach a good trade-off between good reactivity of the system and reduced vibrations and accelerations.

In conclusion, the results demonstrate the significance of both lateral and vertical

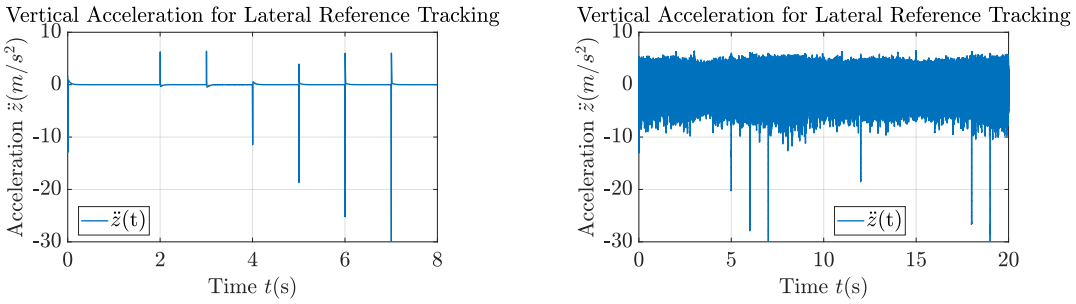

(a) (b)

Fig. 4.4: Results of the simulations for the acceleration in the vertical levitation system subject to the changing reference air-gap of Fig. 4.1. Fig. 4.4(a) shows that the vertical acceleration of the system is zero most of the times and only has instantaneous peaks when a there is a step in the air gap reference. Fig. 4.4(b) shows the effects of the noise on the vertical acceleration, causing it to oscillate over a wider range of values.

accelerations in the Hyperloop system and its relation to the stability, safety and comfort of the passengers or cargo. It is crucial to carefully design and control the guidance and levitation systems to minimize acceleration rates while maintaining stability and safety of the pod, ensuring that the spikes in acceleration are minimized and the structural integrity of the pod is not at risk.

4.3 Power consumption

Power consumption is a crucial aspect of levitation systems as it influences the overall efficiency and cost of operation. In this section, the power consumption of a levitation system is analyzed using SIMULINK simulations. The simulation results provide the current consumption over time for the task of reference tracking. By understanding the current consumption of the system through the use of simulations, it is possible to identify key areas for optimization and improvement to enhance the overall performance of the levitation system. The results in Fig. 4.5(a) demonstrate the correlation between current usage and reference tracking for the guidance system. The graph shows that an increase in the air-gap leads to an increase in the current usage, which is necessary to maintain a straight travel direction and compensate for the loss of guidance force due to the increase in the air-gap. It is also evident that when the reference falls below the equilibrium point, the system utilizes a negative current, indicating that the opposing EMS is activated.

An important trend to note is the effect of measurement noise on the system's performance, as seen in the graph on the right where noise is added to the system. The current usage exhibits a wider oscillation, indicating a less stable operation. It is also

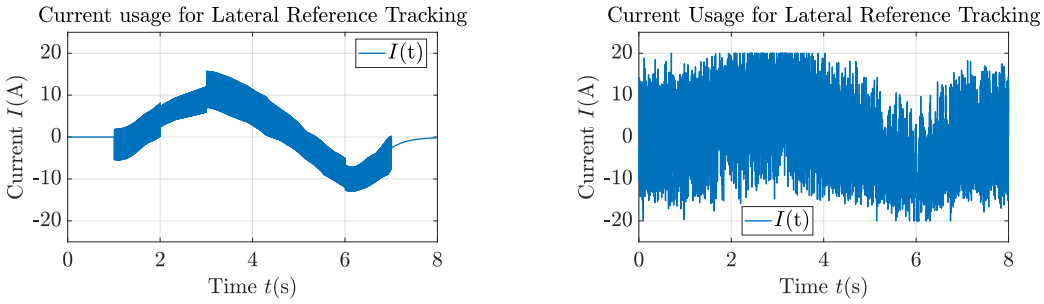

(a) (b)

Fig. 4.5: Results of the simulations for the current consumption in the guidance system subject to the changing reference air-gap of Fig. 4.1. While the simulation for the case without noise, show in Fig. 4.5(a) presents a clear correlation between current usage and reference air gap, when noise is added to the sensor measurement, the current oscillates more, sometimes also reaching the saturation limit ±20 A.

worth mentioning that a wider range of current usage means that the system is operating closer to its limits and thus could compromise the stability and safety of the system. Moreover a wider range means more power loss due to continuous current oscillation and switching between left and right EMS. To better address this issue, the energy used for the reference tracking task of Fig. 4.1 is calculated for the lateral guidance system, and, without the noise is 2482 J for one EMS, which, over a simulation time of 20 s, translates to an average power consumption of 124 W. For the case where the noise is added to the measurement, the energy used amounts to 3732 J, i.e. 187 W, representing a 50% increase in the power usage. The same current behavior is also observed in the simulations for the vertical levitation system.

In summary, the results presented in Fig.4.5 illustrate the relationship between current usage, air-gap, and reference tracking for the guidance system, highlighting the importance of accurate measurements and noise reduction to maintain stability and efficiency. A general remark on the behaviour of the three performance indicator in the case where noise is added to the system is that the increase in oscillation for current and accelerations is most likely caused by the PID controller being too aggressive and by its derivative parameter being too large. Nevertheless, in this case, a large D component is necessary to operate within the tight window of the allowed air gap ranges and avoid excessive overshoot.

Chapter 5

Conclusion

The Hyperloop idea proposes a new mode of transportation that aims to be as energy-efficient as trains and buses, while also offering high-speed travel similar to that of aircrafts. Due to its many theoretical advantages, the Swissloop student team of ETH Zürich works to continually innovate this technology by constructing and upgrading a pod each year.

This thesis aims to improve the Swissloop pod by substituting the traditional suspension and guidance wheels with a magnetic levitation suspension. The focus of the thesis is on the development and design of a control system for the magnetic levitation and guidance of the pod. The proposed control system is created with the intent of ensuring stability, precision and safety during the levitation process.

The main objective of this thesis is to showcase how the system is modeled, and the techniques used to design, test, and validate the control system through simulations in Matlab SIMULINK. The performance metrics examined include the ability of the control system to maintain a constant height above the rail while rejecting external disturbances, the smoothness of the ride, and the current usage required for levitation.

The simulation results of the lateral guidance system show that the system is able to effectively track the reference air-gap, with a maximum overshoot of 0.5 mm, and operate within the safe range of air-gap without engaging the safety wheels. Upon the addition of noisy feedback, the result is an increase in overshoot and deviation from the reference is observed, which is evident in the engagement of the safety wheels.

The simulation results of the vertical levitation system also show similar behavior, where the system is able to maintain stability and track the reference air-gap effectively without noise, but the performance is degraded in the presence of noise. Still, the overshoot remained below 1 mm. The noise added to the measurements is represented by an uniform number in the range -16-16 µm for both the vertical and lateral system. It is based on the sensor information and a safety factor.

The simulation results demonstrate that the presence of noise had an impact on the performance of the proposed control system for both the lateral guidance and vertical levitation systems. The three performance metrics chosen in this thesis - reference tracking, acceleration, and current usage - are all slightly affected by the noise which resulted in increased oscillations in the system's acceleration and current usage, which could lead to energy inefficiencies. Moreover, introducing noise in the system, leads to higher accelerations. Even though the peaks are instantaneous with negligible effects on displacement and speed, they still need further analysis because they could potentially

be dangerous for the pod's structural integrity and the safety of passengers and cargo in the future.

These findings suggest that the proposed control system is able to efficiently maintain stability and to track the reference both with and without the noise maintaining the position of the pod in the allowed range. However, when the measurement is affected by noise, the safety wheels are minimally engaged. This suggest that the operation window may be too tight for real world operation. Thus, future research should focus on increasing the allowed operating range by optimizing the pod structure and try to implement analog as well as digital filter to reduce noise. Additionally, future research should also consider the integration of machine learning techniques to improve the controller's performance and state-estimation techniques to decrease the effect of the noise.

Another important area to focus on is combining the vertical and lateral models into one big model for more realistic simulations. This would allow for a more comprehensive understanding of the interactions between the different components of the levitation system and how they affect overall performance.

Although it is outside the scope of this thesis, the Swissloop team is currently working on building this year pod with the integrated levitation system, which will allow for direct testing and validation of the controller and the levitation system under real-world conditions. This approach also helps to identify any potential issues or limitations that are not captured in the simulation-based thesis.

In conclusion, the results of this thesis demonstrate the effectiveness of the proposed control system in maintaining the stability of the levitation system and improving the tracking performance in a tight operating range under normal and real-world operating conditions.

References

[1] *Climate Change: Evidence and Causes: Update 2020.* Washington, DC: The National Academies Press, 2020.

[2] R. P. Core Writing Team and L. Meyer, "Climate change 2014: Synthesis report. contribution of working groups i, ii and iii to the fifth assessment report of the intergovernmental panel on climate change," *IPCC*, 2014.

[3] D. Banister, "Sustainable transport and public policy," *Trasnport Engeneering and Planning*, vol. 2, pp. 192–214, 2009.

[4] A. Dabrowska, S. de Caluwe, M. Geuze, D. Härtl, R. Roeske, and T. Xydianou, "A pre-project feasibility for connecting noord- and zuid holland via hyperloop," Tech. Rep., 2021.

[5] D. of Energy, "Effect of hyperloop technologies on the electric grid and transportation energy," USDOE Office of Energy Efficiency and Renewable Energy (EERE), Washington, Tech. Rep., 2021.

[6] "Transport and environment report 2020 - train or plane?" European Environment Agency, Tech. Rep., 2020.

[7] E. Musk, "Hyperloop alpha - tesla," 2013. [Online]. Available: https://www.tesla.com/sites/default/files/blog_images/hyperloop-alpha.pdf

[8] R. Thornton, "The future of maglev," in *2007 International Conference on Electrical Machines and Systems (ICEMS)*, 2007, pp. 1950–1954.

[9] T. Luu and D. Nguyen, "Maglev: The train of the future," in *Fifth Annual Freshman Conference, Tesla Society, Paper*, vol. 270, 2005.

[10] W. Chao and W. Kang, "A study on environmental impact of high speed maglev traffic engineering," *2010 International Conference on Management and Service Science, MASS 2010*, 08 2010.

[11] W. Cornell, "Maglev: Magnetic levitating trains." [Online]. Available: https://sites.tufts.edu/eeseniordesignhandbook/2015/maglev-magnetic-levitating-trains/

[12] H.-W. Lee, K.-C. Kim, and J. Lee, "Review of maglev train technologies," *IEEE Transactions on Magnetics*, vol. 42, no. 7, pp. 1917–1925, 2006.

[13] D. Bortis, *Magnetic Circuit*, ser. Lecture notes in Fundamentals of Electric Machines. Power Electronic System Laboratory at ETH Zurich, 2022.

[14] L. Guzzella, *Analysis and synthesis of Single-input Single-output control systems.* vdf Hochschulverlag AG, 2011.

[15] "Hardt - the hyperloop." [Online]. Available: https://hardt.global/hyperloop-system

[16] L. Guzzella, *Discrete Time Control Systems*, ser. Lecture notes of Digital Control System. Institute for Dynamic System and Control at ETH Zurich, 2013.